Supplements to: Representation of polynyas in the Ross Sea coupled atmosphere—sea ice—ocean model P-SKRIPSv2

Alexandra Gossart¹, Alena Malyarenko², Liv Cornelissen^{3,4}, Craig Stevens^{3,4}, Una Miller⁵, Christopher J. Zappa⁶, Nancy Lucà⁷, Pasquale Castagno⁸, and Giorgio Budillon⁹

Correspondence: Alexandra Gossart (alexandra.gossart@vuw.ac.nz)

S1 Datasets

S1.1 Satellite Data

S1.1.1 AMSR - Sea ice concentration

We use the daily sea ice concentration product AMSR2 at 3.125 km grid spacing, available since 2012 (ver 5.4; Melsheimer and Spreen (2019)). This dataset, referred to as AMSR in this paper, estimates sea ice concentrations from the microwave radiometer brightness temperature data of the Advanced Microwave Scanning Radiometer 2 on the JAXA satellite GCOM-W1, using the ARTIST Sea Ice algorithm (Spreen et al., 2008). The data is available at https://data.seaice.uni-bremen.de/amsr2/asi_daygrid swath/s3125/2018/jun/Antarctic3125/ (last accessed = 06/2024).

S1.1.2 SSMI - Sea ice concentration

Another SIC dataset is produced from the Special Sensor Microwave/Imager (SSM/I) and Special Sensor Microwave/Image Sounder (SSM/IS). This dataset is referred to as SSMI hereafter. The grid resolution is 12.5 km and the ARTISTS Sea Ice algorithm (Kaleschke et al., 2001; Spreen et al., 2008) is also used to convert brightness temperatures, but applied to channels enabling finer resolution (85 GHz), to which a 5 days median filter is applied to get rid of weather biases (e.g. Kern et al., 2010). The daily data is available at https://www.cen.uni-hamburg.de/en/icdc/data/cryosphere/seaiceconcentration-asi-ssmi.html for the 1991-2023 time period on the NSIDC grid (DiGirolamo et al., 2022), (last accessed = 06/2024).

¹Te Puna Pātiotio | Antarctic Research Centre, Te Herenga Waka | Victoria University of Wellington, Te Whanganui a Tara | Wellington, Aotearoa | New Zealand

²Te Kura Aronukurangi | School of Earth and Environment, Te Rāngai Pūtaiao | College of Science, Whare Wānanga o Waitaha | University of Canterbury, Ōtautahi | Christchurch, Aotearoa | New Zealand

³Ocean Physics Group, Earth Sciences New Zealand, Te Whanganui a Tara | Wellington, Aotearoa | New Zealand

⁴Te Kura Mātai Ahupūngao | Department of Physics, Waipapa Taumata Rau | University of Auckland, Tāmaki Makaurau | Auckland, Aotearoa | New Zealand

⁵Graduate School of Oceanography, University of Rhode Island, Narragansett, RI, USA

⁶Lamont Doherty Earth Observatory of Columbia University, Palisades, NY, USA

⁷Università Ca' Foscari Venezia, Università degli Studi di Napoli 'Parthenope', Italy

⁸Università degli Studi di Messina, Italy

S1.1.3 Bootstrap - Sea ice concentration

We use the daily Bootstrap Sea Ice Concentrations dataset from NSIDC (National Snow and Ice Data Centre), derived from measurements from the Scanning Multichannel Microwave Radiometer and the Special Sensor Microwave/Imager on the Nimbus-7 and DMSO-F10 satellites, respectively. The sea ice cover is generated using the Advanced Microwave Scanning Radiometer - Earth Observing System (AMSR-E) Bootstrap Algorithm on a polar stereographic grid (25 x 25 km). This data is available from the 1st of November 1978 until the end of 2022 at https://nsidc.org/data/nsidc-0079/versions/3 (Comiso, 2017) and called Bootstrap in this paper, (last accessed = 06/2024).

S1.1.4 CryoSat-2 - Sea ice concentration and sea ice thickness

We use the Antarctic Sea Ice Thickness Estimates from CryoSat-2 available here: https://zenodo.org/record/7327711#.ZGWsc ZFBz0p which contains SIC and sea ice thickness estimates using snow depth and snow freeboard retrieved from CryoSat-2 Synthetic Aperture Radar altimeter using the Baseline-D Level 1b waveform data (Fons et al., 2023). The dataset is available monthly for 2010-2021 and includes georeferenced snow depth on sea ice, snow freeboard, ice freeboard and the derived sea ice thickness and estimated uncertainty. The data is generated using the CryoSat-2 Waveform-Fitting method for Antarctic sea ice (CS2WFA) (last accessed = 06/2024).

80 S1.1.5 SMOS - sea ice thickness

The SMOS (ESA's Soil Moisture and Ocean Salinity mission) Level 3 Sea Ice Thickness dataset (SMOS hereafter) also provides estimates of thin sea ice thickness and its uncertainty from 2010 onwards at daily temporal resolution for the austral winter (15/04 to 15/10 each year) at 12.5 km spatial resolution (Kaleschke et al., 2012, 2023). The retrieval is based on the v620 SMOS L1C product and can derive up to 1.5 m ice thickness information from daily averaged brightness temperature. The data is available on Pangaea at https://doi.org/10.1594/PANGAEA.934732 (last accessed= 31/07/2024).

S1.1.6 NOAA - sea ice concentration

The SIC data used in this study to compare to our model output come from the NOAA DOISST v2.1 data set, a daily mean product with 0.25° spatial resolution (referred to as NOOA in this paper; Huang et al. (2021)). This dataset combines argo, buoys and in situ ship measurement of SST with satellite-derived observations from the Advanced Very High Resolution Radiometer (AVHRR) and shows some improvements in the treatment of winter SST in the Antarctic compared to the previous version (v2.0). The dataset covers the period from 1981 to present and can be found at https://www.ncei.noaa.gov/data/sea-surface-temperature-optimum-interpolation/v2.1/access/avhrr/ (last accessed = 01/2024).

S1.2 Reanalyses and model outputs

S1.2.1 AMPS model output

We incorporate the Antarctic Mesoscale Prediction System (AMPS) data to the comparison. AMPS is a numerical weather prediction model, using the WRF physical core (Polar MM5) and the Model for Prediction Across Scales (MPAS) to produce Antarctic prediction twice daily, developed by the National Center for Atmospheric Research (NCAR) and the Byrd Polar Research Centre at Ohio State University (Powers et al., 2003). We use the high resolution outputs from the grid 3 (Ross Sea at 2.67km, https://www2.mmm.ucar.edu/rt/amps/information/configuration/configuration.html).

0 S1.2.2 Glorys Ocean Reanalysis

Glorys12v1 (Gasparin et al. (2021), Glorys hereafter) is a gridded global reanalysis product developed in the frame of the European Copernicus Marine Environment Monitoring Service (CMEMS). It provides state-of-the-art daily and monthly estimates of temperature, salinity, current speed and direction and sea level, as well as sea ice extent, concentration and thickness at 1/12th of degree and on 50 vertical levels (eddy-permitting). The model is the Nucleus for European Modelling of the Ocean platform (Madec and Team, 2008) which comprises the Ocean Parallélisé (OPA) model, coupled to the LIM2 sea ice model (Fichefet and Maqueda, 1997). It is forced at the surface by atmospheric ECMWF reanalysis (Dee et al., 2014) and assimilates observed local temperature and salinity profiles, satellite sea surface temperature observations and along track surface level anomaly information derived from satellite altimetry. The temporal coverage of the dataset is from 1993 onward.

S1.2.3 ORAS5 reanalysis

The Ocean ReAnalysis System 5 (ORAS5; Zuo et al. (2019) is a gridded global product presenting an historical estimate of the ocean state from 1979 until present day produced by the ECMWF at eddy-permitting horizontal resolution (1/4 degree) and 75 levels. It consists of 5 ensemble members and comprises a prognostic thermodynamic-dynamic sea ice model that assimilates sea ice concentration data as well as in-situ observations of salinity and temperature profiles and altimetry along-track observations of sea level anomalies and is nudged towards sea surface temperature observations. Similarly to the GLORYS reanalysis, the numerical core is based on NEMO v3.4.1 ocean model (Madec and Team, 2008) that includes the LIM2 sea ice model (Fichefet and Maqueda, 1997) and is forced by the ERA-Interim ECMWF atmospheric reanalysis (Dee et al., 2011). In addition, the 5 members are varied by perturbing the initial conditions, the forcings, and the observations. Uotila et al. (2019) indicated that the Antarctic sea ice is well represented in this reanalysis.

S1.3 Point locations and World Ocean Atlas

70 S1.3.1 World Ocean Atlas - Temperature and salinity

We use the temperature and salinity datasets from the World Ocean Atlas (WOA, Reagan et al. (2024)) global database at 1/4 degree for the year 2017. These are quality checked monthly mean observations and standard depth data profiles, a gridded

product derived at the Ocean Climate Laboratory of the National Oceanographic Data Center from the World Ocean Database and are available for the period 1770 to 2018. The World Ocean Atlas is widely used in oceanographic studies and is a recognised dataset.

S1.3.2 AWS - Meteorological data

We compare the PWRF basic meteorological variables to automatic weather station measurements from the ANTAWS dataset (3-hourly data, Wang et al. (2023)) at the Vito and Manuela stations (Figure 1 b)). We evaluate the 2m temperature and relative humidity, surface pressure and 10 m wind speed from the corresponding model grid cell. We correct the temperature by applying a dry adiabatic lapse rate of $9.8^{\circ}Ckm^{-1}$ (Bromwich and Fogt, 2004) to account for discrepancies between the modelled grid cell elevation and the actual station elevation. In addition, we extrapolate the observed wind speed from 2m to 10m according to Sanz Rodrigo (2011). Vito AWS [78.408 ° S, 177.829° E] was selected as it is located close to the edge of the Ross ice shelf, where the winds blow offshore and open up the RSP. The elevation of the station is 50 m, which is the same elevation as the closest P-SKRIPS model grid cell. The station has been recording since 2004. The other station investigated in this paper is Manuela, placed upstream of the TNBP in complex terrain. Manuela was established in 1984 [74.946 °S, 163.687° E]. The closest model grid cell has an elevation of 12 m agl while the real AWS station lies at 78 m asl.

S1.3.3 Multiparameter PIPERS voyage dataset

The PIPERS (Polynyas and Ice Production in the Ross Sea, U.S. Antarctic Program Data Center, https://www.usap-dc.org/view/project/p0010032 last accessed:30/05/2024) was a multi-institutional project with the aim to estimate the sea ice production and water masses transformation in the Ross Sea. This project led an oceanic cruise into the polynyas of the Ross Sea in 2017 (11th of April to 10th of June - austral fall season). The cruise was equipped with state-of-the-art unmanned instruments such as UASs (Unmanned Airborne Systems), AUVs (Autonomous Underwater Vehicles) and ROVs (Remotely Operated Underwater Vehicles) that sampled concurrently the ocean, sea ice and atmosphere. The data used in this study are the Vertical CTD profiles conducted by Thompson et al. (2020) (red star in Figure 1 c)), that span the katabatic events between 04 and 11th of May 2017 within the RSP (https://www.usap-dc.org/view/dataset/601192), and the rawinsondes profiles as well as meteorological data onboard the ship (https://www.usap-dc.org/view/project/p0010032), corresponding to the same dates (yellow dots in Figure 1 b)). We refer to these datasets as PIPERS hereafter.

S1.3.4 Hydrographic timeseries - DITx dataset

DITx consists of a long mooring, DITN located close to the DIT [75.36 ° S, 164.746° W], and a short mooring in the deepest part of the Drygalski Trough [75.276 °S, 164.067 °W] (yellow stars in Figure 1 c)). The time series started in December 2014 with DITN, and DITD was added in February 2017. DITN consists of 3 pairs of CTD (SBE37SM) and Aquadopp current profilers at \sim 75, 275 and 670m depth and an array of thermistors in 2017 at \sim 200, 330 and 360m depth. The full dataset of the DITx moorings are described in Cornelissen et al [in prep] and are available through the Korea Polar Data Centre.

S1.3.5 Hydrographic timeseries - LDEO dataset

The Lamont-Doherty Earth Observatory (LDEO) mooring was deployed from February 2017 - 2018 near the face of the Nansen Ice Shelf, in the region of active HSSW formation. It was deployed in 390 m water depth with instrumentation that included 7 temperature-salinity sensors at depths ranging from 47 to 360 m.

S1.3.6 Hydrographic timeseries - MORSea Mooring D

This dataset is derived from the MORSea oceanographic mooring "Mooring D" [75°08.1666' S, 164°35.3748' E] deployed during the PNRA XXXII Expedition (2016/17) on 11 February 2017 and recovered during the PNRA XXXIV Expedition (2018/19) on 19 February 2019. The mooring was positioned at a depth of 1144 meters. The following instruments were mounted along the mooring line, listed from shallowest to deepest: SBE16 at 556 m, recording temperature and salinity at a 30 minute sampling interval. SBE37 at 772 m, recording temperature and salinity at a 30 minute sampling interval. Aanderaa Seaguard at 911 m, recording current velocity components (*U*, *V*), speed, and direction at a 30 minute sampling interval. SBE39 at 996 m, recording temperature at a 30 minute sampling interval. SBE37 at 1086 m, recording temperature and salinity at a 30 minute sampling interval. Aanderaa Seaguard at 1135 m, recording *U*, *V*, speed, and direction at a 30 minute sampling interval.

Table S1. Annual SIC [0-1] mean value \pm standard deviation for each of the domains (displayed in Figure 1 - Terra Nova Bay polynya (TNBP) - Ross Sea Polynya (RSP) and the Open Ocean (OO), annually and for each season.

		cryosat	NOOA	Glorys	ORA	Bootstrap	SMMI	AMSR	sim 001	sim 002	sim 003
year	TNB	0.65±0.19	-	0.71±0.25	0.53±0.26	0.67±0.21	0.56±0.3	0.79 ± 0.3	0.50 ± 0.29	0.36±0.23	0.30±0.21
	RSP	0.6 ± 0.3	-	0.52 ± 0.26	0.4 ± 0.22	0.6 ± 0.33	0.58 ± 0.34	0.74 ± 0.37	0.43 ± 0.25	$0.35 {\pm} 0.22$	0.32 ± 0.21
	OO	0.76 ± 0.35	0.69 ± 0.39	0.82 ± 0.26	0.73 ± 0.33	0.77 ± 0.35	0.73 ± 0.34	0.82 ± 0.36	0.69 ± 0.37	0.64 ± 0.39	0.58 ± 0.4
MAM	TNB	0.64±0.2	-	0.67±0.24	0.51±0.1	0.66±0.08	0.53±0.13	0.97±0.03	0.40±0.22	0.31±0.17	0.28±0.16
	RSP	0.6 ± 0.31	-	$0,41\pm0.23$	0.41 ± 0.12	0.64 ± 0.25	0.62 ± 0.26	0.97 ± 0.04	0.44 ± 0.17	0.37 ± 0.14	0.33 ± 0.13
	OO	0.76 ± 0.35	0.6 ± 0.41	0.69 ± 0.36	0.66 ± 0.35	0.7 ± 0.4	0.65 ± 0.39	0.99 ± 0.01	0.5 ± 0.41	0.5 ± 0.4	0.49 ± 0.39
JJA	TNB	0.74±0.02	-	0.83±0.07	0.67±0.01	0.77±0.08	0.77±0.1	0.89±0.21	0.69±0.09	0.54±0.1	0.48±0.1
	RSP	0.79 ± 0.02	-	0.62 ± 0.15	0.55 ± 0.03	0.8 ± 0.08	0.82 ± 0.08	0.88 ± 0.19	0.63 ± 0.04	0.54 ± 0.05	0.5 ± 006
	OO	0.97 ± 0.01	0.95 ± 0.03	0.94 ± 0.02	0.93 ± 0.01	0.97 ± 0.03	0.93 ± 0.04	0.99 ± 0.01	0.94 ± 0.01	0.92 ± 0.01	0.9 ± 0.02
SON	TNB	0.79±0.06	-	0.78±0.2	0.67±0.09	0.81±0.12	0.7±0.24	0.89±0.21	0.68±0.16	0.41±0.2	0.32±0.19
	RSP	0.76 ± 0.07	-	0.57 ± 0.27	0.49 ± 0.12	0.85 ± 0.17	0.68 ± 0.23	0.88 ± 0.19	0.5 ± 0.18	0.36 ± 0.2	0.32 ± 0.19
	OO	0.94 ± 0.02	0.9 ± 0.06	0.91 ± 0.04	0.9 ± 0.02	0.94 ± 0.04	0.9 ± 0.05	0.99 ± 0.01	0.91 ± 0.04	0.86 ± 0.1	0.71 ± 0.28
D	TNB	0.79±0.06	-	0.21±0.15	0.28±0	0.48±0.06	0.04±0.04	0.23±0.11	0.11±0.05	0.07±0.06	0.02±0.02
	RSP	0.76 ± 0.08	-	-	0.0 ± 0	0.01 ± 0.01	0 ± 0	0.05 ± 0.01	0.009 ± 0.009	0 ± 0	0
	OO	0.94 ± 0.02	0.21 ± 0.32	0.49 ± 0.2	0.5±0	0.56 ± 0.15	0.5 ± 0.11	0.74 ± 0.14	0.54 ± 0.21	0.13 ± 0.12	0

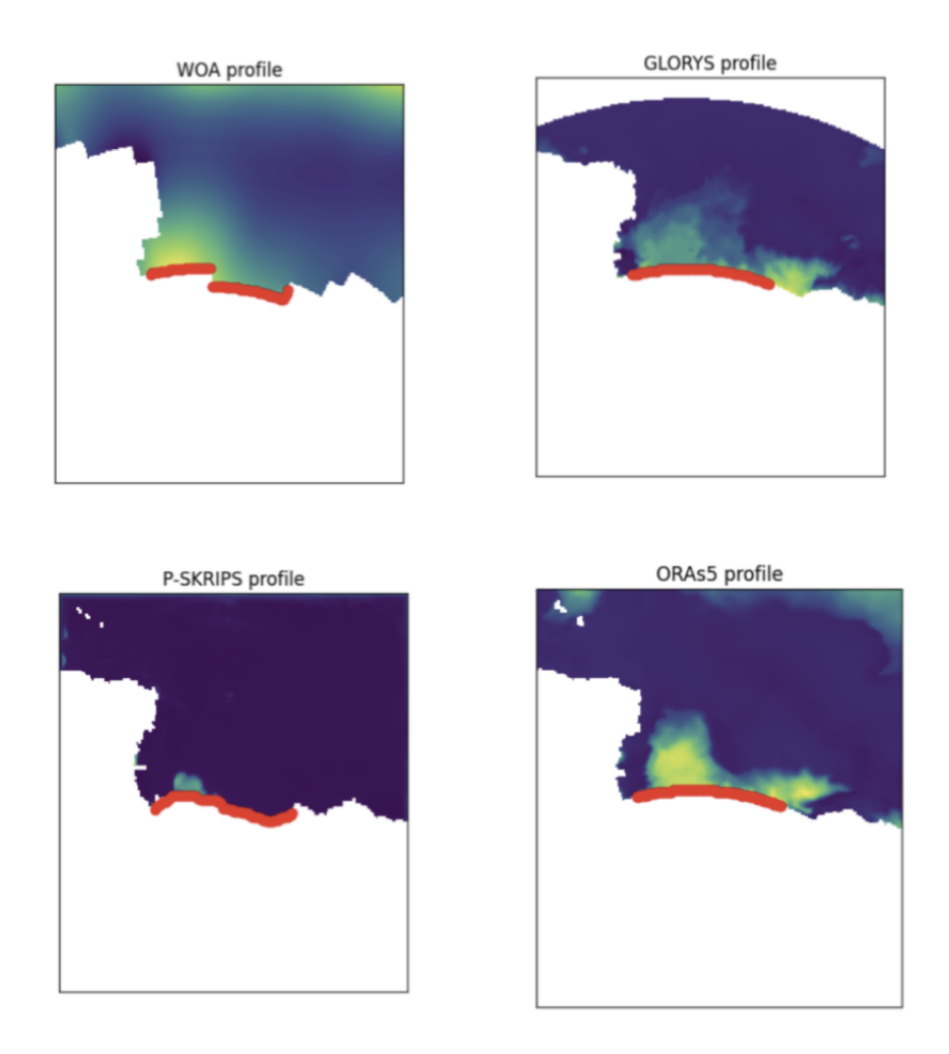


Fig. S1. location of the vertical ocean sections along the ice shelf front, for the different datasets: World Ocean Atlas (top left), GLORYS reanalysis (top right), P-SKRIPS model output (bottom left) and ORAs5 (bottom right). The locations of the profiles are indicated in red. The shading corresponds to ocean surface temperature but only plotted as indicative of where the ocean (color) and land (white) lie.

Table S2. Annual SIT [m] mean value \pm standard deviation for each of the domains (displayed in Figure 1 - Terra Nova Bay polynya (TNBP) - Ross Sea Polynya (RSP) and the Open Ocean (OO), annually and for each season.

		cryosat	SMOS	Glorys	ORA	sim 001	sim 002	sim 003
year	TNB	1.0±0.44	0.23±0.12	0.68±0.27	0.57±0.21	0.61±0.23	0.57±0.23	0.52±0.17
	RSP	1.01 ± 0.09	0.18 ± 0.06	0.48 ± 0.12	0.42 ± 0.2	0.47 ± 0.11	0.41 ± 0.11	0.40 ± 0.11
	OO	1.03 ± 0.14	1.06 ± 0.23	0.57 ± 0.16	0.57 ± 0.25	0.61 ± 0.12	0.64 ± 0.39	0.45 ± 0.09
MAM	TNB	0.72 ± 0.13	0.14±0.04	0.48 ± 0.14	0.52±0.1	0.41 ± 0.1	0.39 ± 0.1	0.38 ± 0.1
	RSP	0.93 ± 0.05	0.13 ± 0.03	0.49 ± 0.07	0.5 ± 0.02	0.39 ± 0.07	0.36 ± 0.06	0.36 ± 0.06
	OO	0.86 ± 0.04	0.97 ± 0.3	0.52 ± 0.14	0.52 ± 0.17	0.45 ± 0.12	0.45 ± 0.1	0.43 ± 0.1
	TNB	1.12±0.14	0.22±0.06	0.68 ± 0.05	0.58±0.01	0.54±0.05	0.52±0.06	0.52 ± 0.06
JJA	RSP	1.05 ± 0.04	0.19 ± 0.06	0.53 ± 0.02	0.53 ± 0.01	0.52 ± 0.05	0.47 ± 0.03	0.47 ± 0.03
	OO	1.05 ± 0.03	1.13 ± 0.17	0.71 ± 0.04	0.81 ± 0.01	0.69 ± 0.04	0.57 ± 0.03	0.48 ± 0.05
	TNB	1.42±0.38	0.33±0.17	0.97±0.22	0.8 ± 0.17	0.83±0.25	0.77±0.26	0.64±0.2
SON	RSP	1.04 ± 0.1	0.22 ± 0.07	0.46 ± 0.15	0.48 ± 0.07	0.05 ± 0.09	0.43 ± 0.13	0.42 ± 0.13
	OO	1.14 ± 0.13	0.99 ± 0.18	0.56 ± 0.09	0.64 ± 0.09	0.68 ± 0.02	0.52 ± 0.05	0.42 ± 0.11
	TNB	0.26±0	-	0.34±0.13	0.47±0	0.72±0.16	0.62±0.24	0.49±0.13
D	RSP	-	-	-	0 ± 0	0.16 ± 0.14	0.27 ± 0.12	0.25 ± 0.1
	OO	1.12±0	-	0.49 ± 0.1	0.4 ± 0	0.53 ± 0.08	0.28 ± 0.1	-

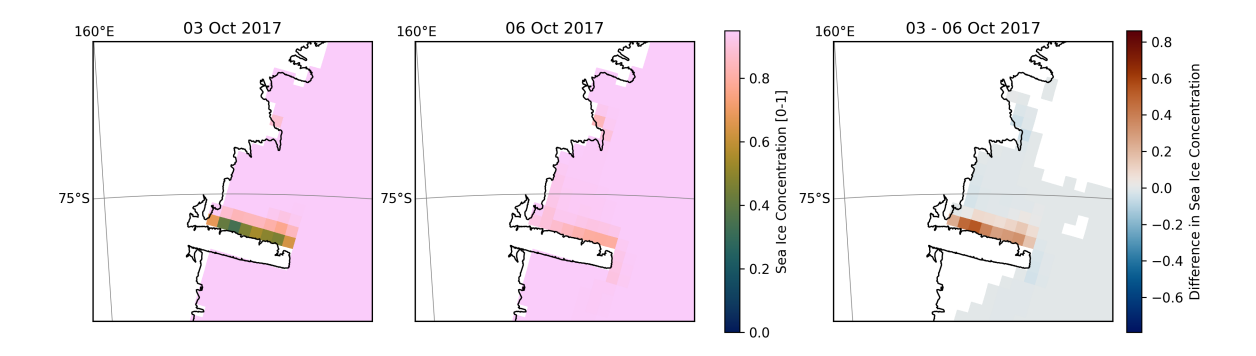


Fig. S2. Sea ice concentration change for event 3: The storms and onshore winds close off the TNB polynya between the 3rd and 6th of October 2017.

S2 Atmosphere comparison

The temperature variations are very similar for the three datasets, indicating that both models perform well in front of the RSP (Figure S4 and S5) although a slightly cold bias is visible in the modelled simulations, compared to the AWS measurements:

P-SKRIPS and AMPS are slightly skewed to the left (peaks at -36 and -39, respectively) compared to the AWS dataset that peaks at -24 °C. The WI reaches 0.76 and 0.81, the highest scores at this location. At Vito station, both AMPS and P-SKRIPS perform quasi equally and slightly underestimate the relative humidity throughout the year, which means a dry bias of 14%

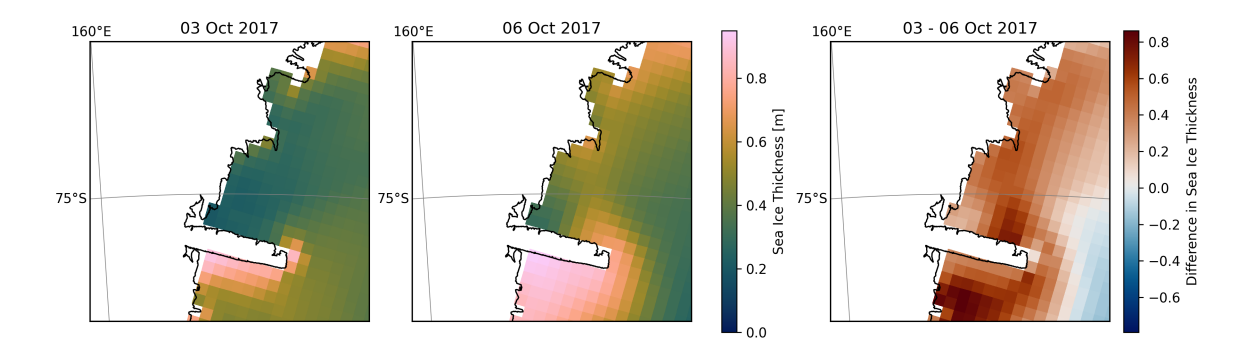


Fig. S3. Sea ice thickness change for event 3: the storms and onshore winds pile up the sea ice in the TNB polynya along the DIT between the 3rd and 6th of October 2017.

in the model outputs (Figure S4 and Table 2), until early November. Then the models display larger values than measured at the station for the last two months, visible as the small peak in the distribution between 80 and 90%. The wind speed is overestimated by both AMPS and P-SKRIPS over the whole time period (RMSE of 4 and $3m.s^{-1}$, respectively). This is clear in both Figures 5 and 6, and Figures S4 and S5: the mean values and the extremes reach larger intensities in model outputs, compared to the measured wind speeds and P-SKRIPS has the largest discrepancy to the observations (WI of 0.41 - P-SKRIPS and 0.53 - AMPS). The direction of the wind, however, is rather well represented by the models which means that both the local effects, but also the large-scale circulation are taken into account in the simulations. It is encouraging to see that both wind speed and direction are well aligned, as these are common model struggles and an important driver of polynya activity. Finally, the variations of the pressure field are similar for the three datasets.

130

135

140

Figure S6 illustrates the fairly good match between the model output cells closest to the coordinates of the ship at the measurement time, and the observations taken onboard the PIPERS ship during its journey in the Ross Sea between mid-April until the beginning of May 2017 (yellow dots in Figure 1 b)). After assessing P-SKRIPS performance over land in section 3.3, this comparison enables us to evaluate the performance of the atmosphere component of P-SKRIPS over the ocean within the Ross Sea. The 2 m temperature is in turn over- and underestimated by the two models, and overall P-SKRIPS is closer to the observed values than the AMPS prediction. Both models start off colder than the observations on the 14th of April but the three curves converge during the next week and have similar magnitudes and variability. The warming event picked up in the observations around the 20th of May is absent in both simulations, but the rest of the fluctuations are simulated by the models well. From the 18th of May, the simulations diverge clearly and only reconcile around the 28th and 30th, when the AMPS output suddenly warms and reaches the higher temperatures of the ship and P-SKRIPS. Between the 18th and 28th of May, P-SKRIPS lies really close to the observations, then tends to overestimate the temperature slightly. The surface pressure is well simulated, albeit better by AMPS than PWRF, that tends to overestimate the pressure over the whole time period. Both models perform equally regarding the wind direction, in turns following the sharp changes picked up in the observations

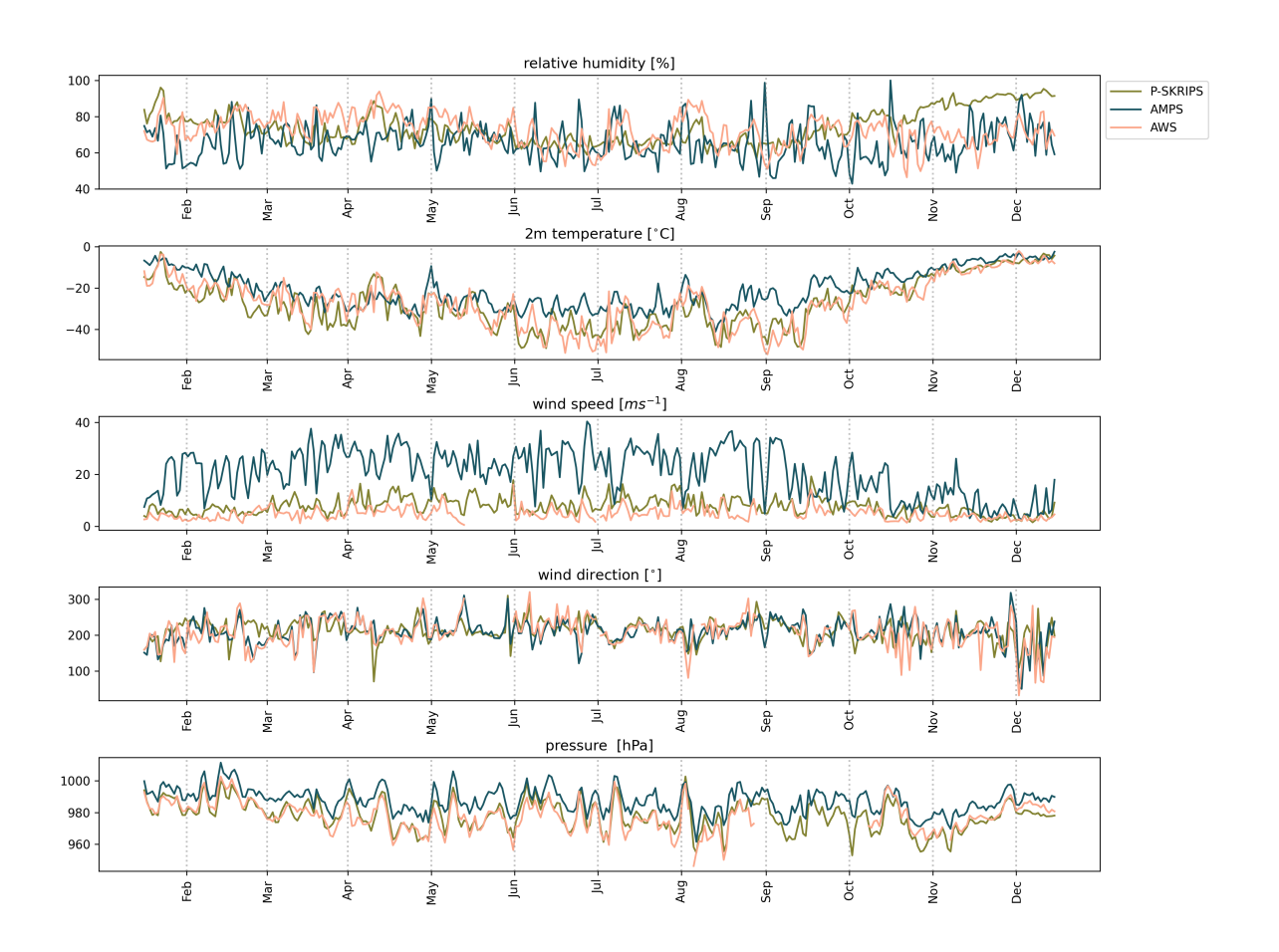
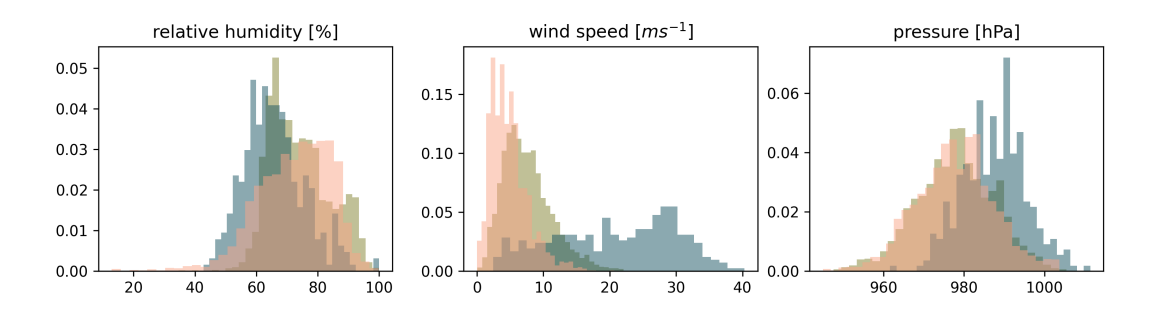


Fig. S4. Timeseries of five meteorological variables at Vito station, February until December 2017, P-SKRIPS sim 002 closest grid cell (5.1 km, same elevation), AMPS model grid cell and AWS data.



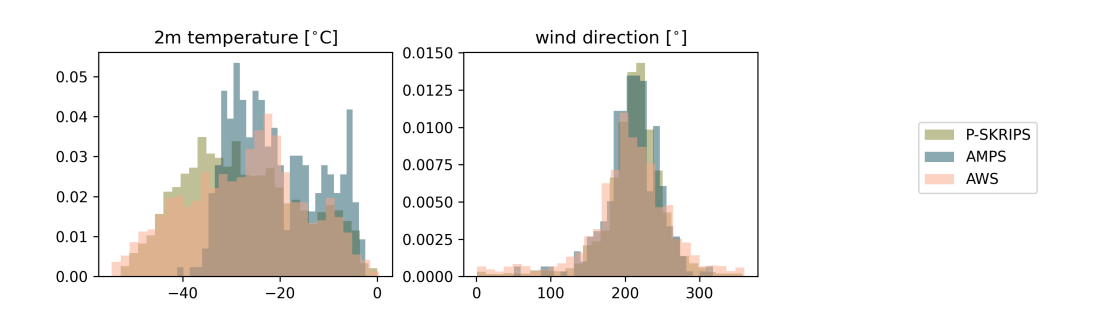


Fig. S5. Same data as in Figure S4, but in the form of distribution. For simplicity, we show only one model simulation (sim 002, khaki) as all the model outputs are very close to each other. The AMPS dataset is in pink and the AWS data is in blue. The vertical lines denote the 15th of each month.

145 (20/04, 26/04, 28/05 and 06/06) but struggle during other events (10 and 14/05 and 30/05). They generally represent the predominance in southeasterlies and southerly winds well between the 30th of April and 27th of May. Finally, the wind speed is only overestimated by the models circa 9th to 12th of May (and 14th to 17th for P-SKRIPS only). The larger wind speeds event caught by the ship in early May lasts a bit longer in the models than in reality, but the magnitude of the winds during the rest of the journey is very similar, compared to the observations.

150 S3 Ocean comparison

155

S3.1 Ocean response along the Ross Ice Shelf (December)

During summer, Simulations 001 to 003 are closest to the WOA salinity pattern in Figure S10. The East-West gradient is still visible but the vertical mixing around 178° W has disappeared. The surface of the ERS is more saline as the drag coefficient increases. The observations (WOA) have smoother isohalines and the 'L' shape is dampened. ORAs5 displays a similar profile to June in the ERS, and the surface water is very fresh beyond 185° and reaches ~200m below the surface. This is totally

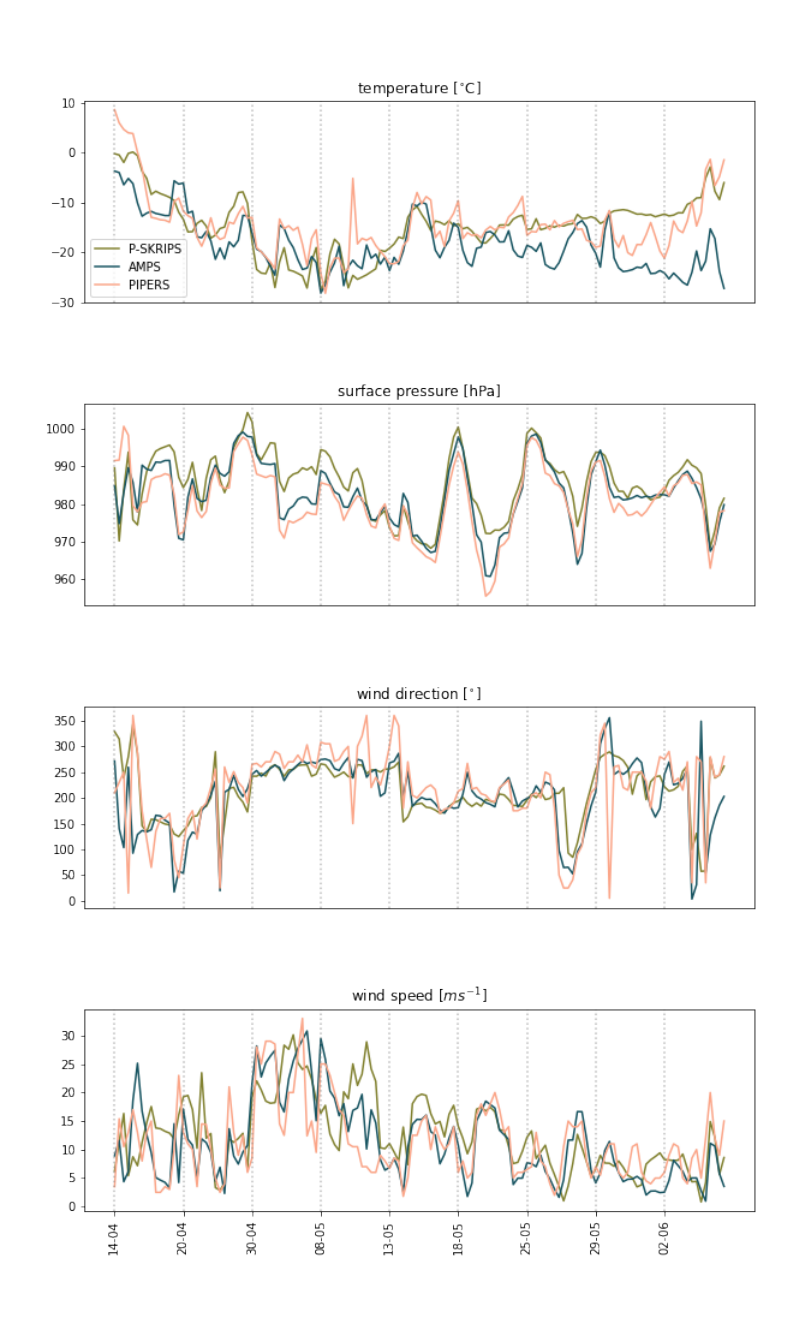


Fig. S6. PIPERS:P-SKRIPS comparison. Time Series of 2m temperature, surface pressure, wind direction and wind speed during the journey of the PIPERS ship in the Ross sea (mid-April to beginning of June 2017, pink) compared to the closest grid cell at each measurement time in P-SKRIPS (khaki) and AMPS (blue).

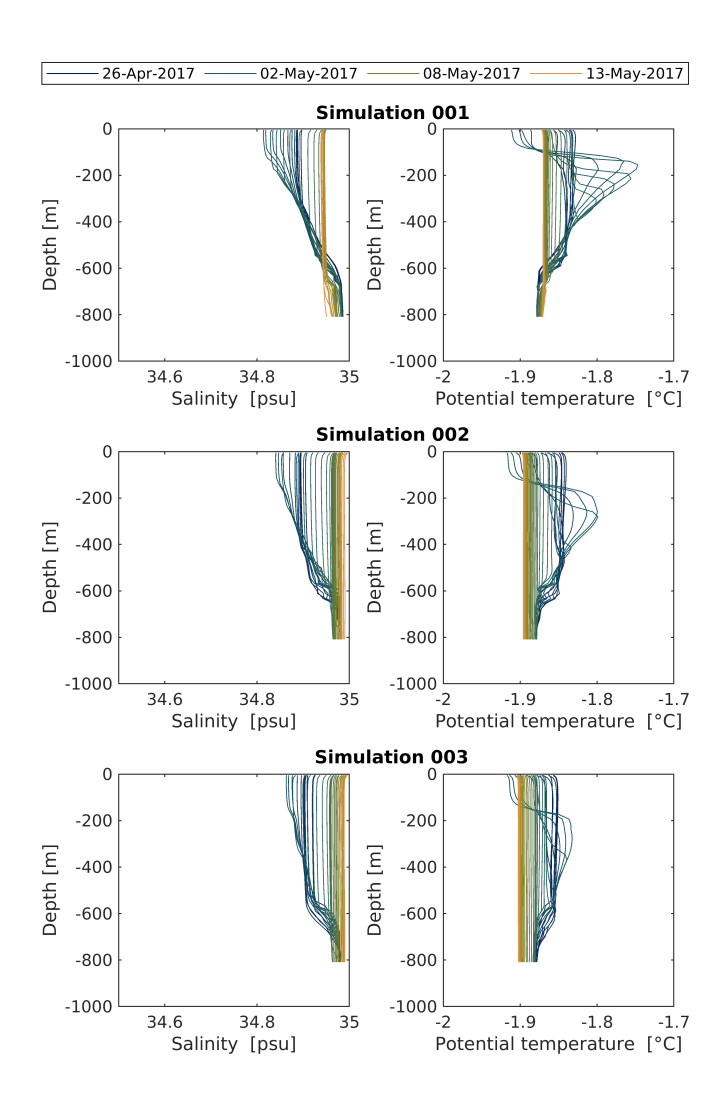


Fig. S7. P-SKRIPS model simulations at the location of the CTD profiles of the ocean performed during the PIPERS cruise, simulation 001 (top row), 002 (middle row) and 003 (bottom row). The first column displays the salinity profiles, the second shows the ocean temperature. The color represents the date at which the profile was sampled.

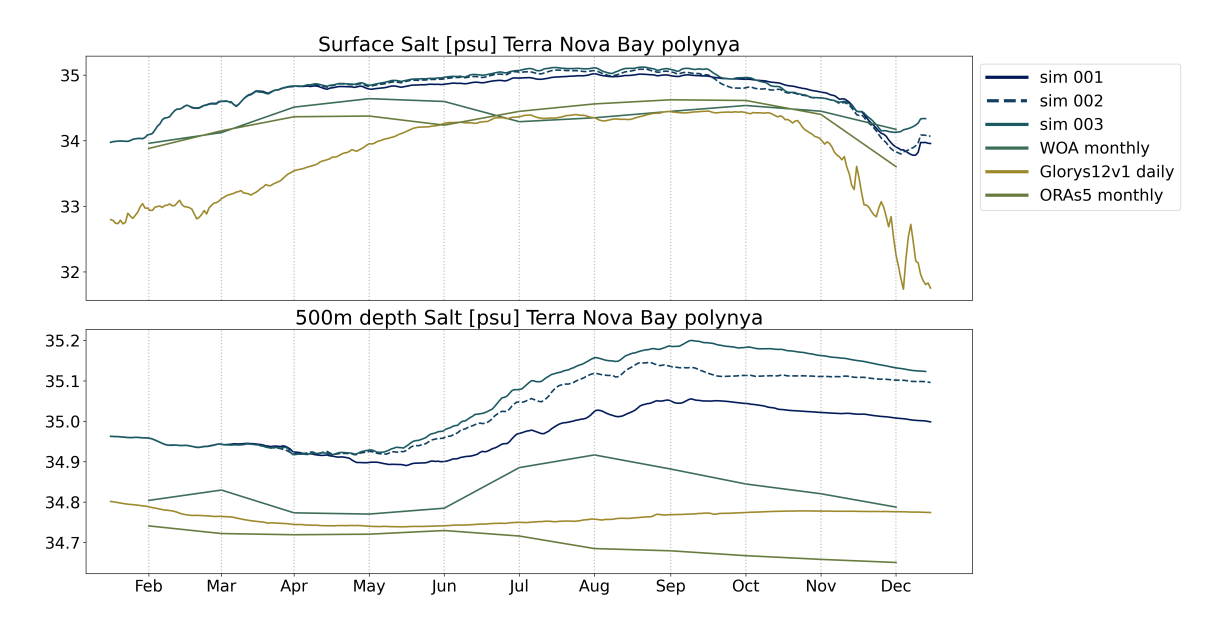


Fig. S8. Time series of the spatial mean salinity at the surface (top) and at 500 m depth (bottom) in the TNBP box.

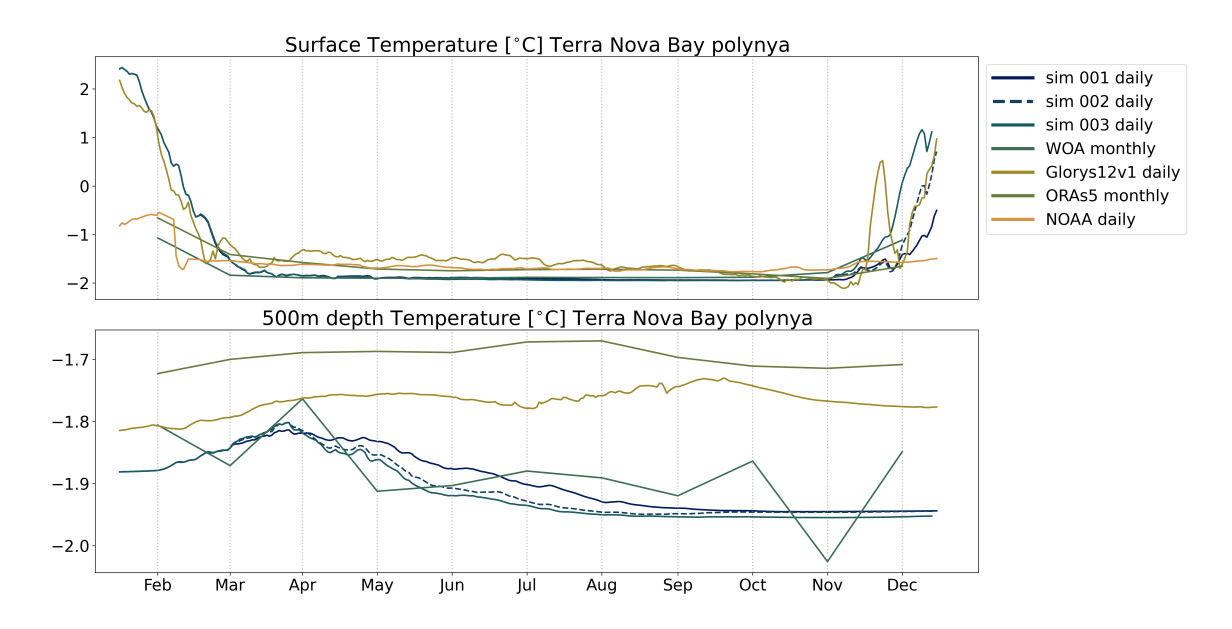


Fig. S9. Time series of the spatial mean temperature at the surface (top) and at 500 m depth (bottom) in the TNBP box.

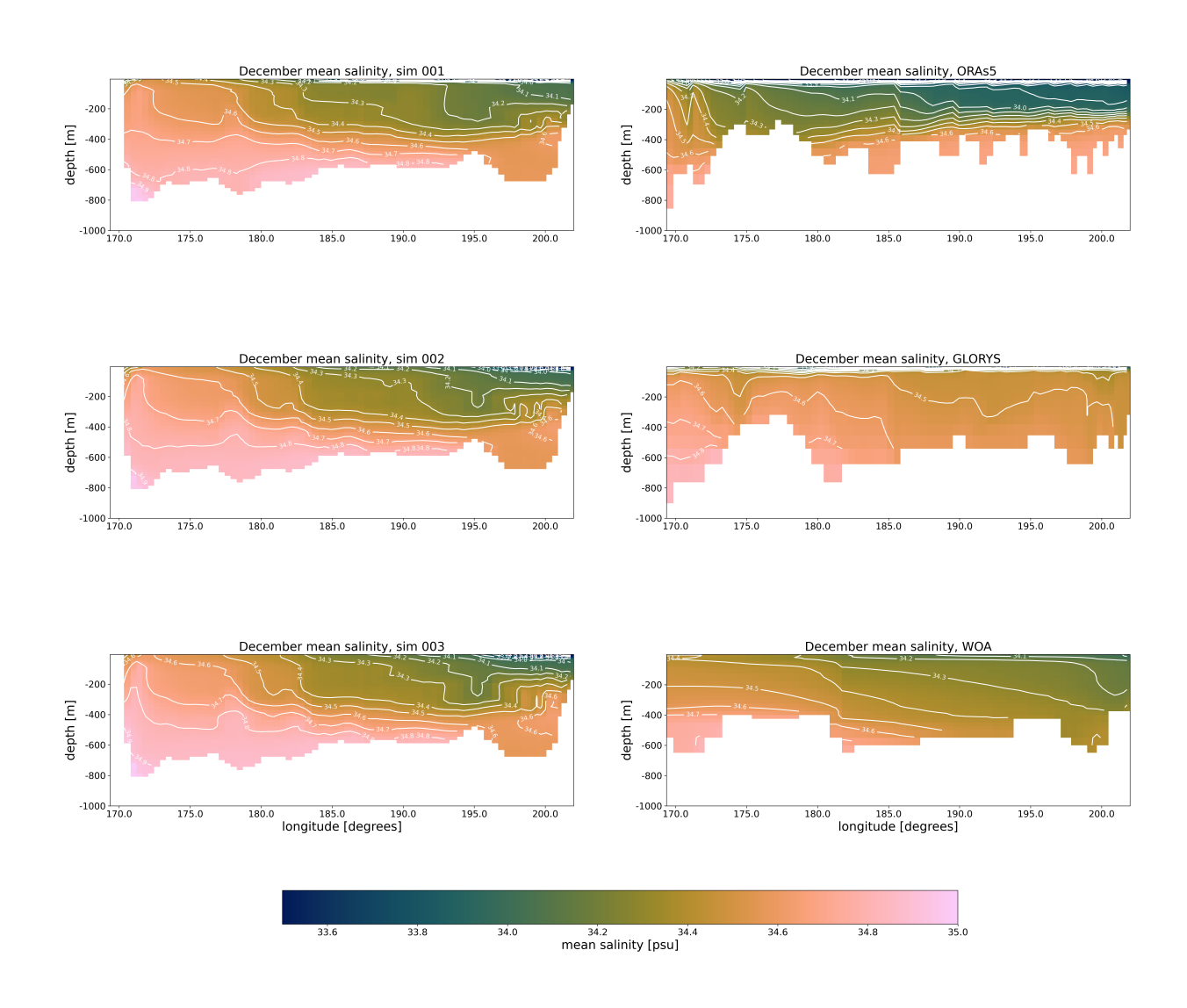


Fig. S10. Salinity profiles and contours along the ice shelf edge, monthly mean values for December 2017.

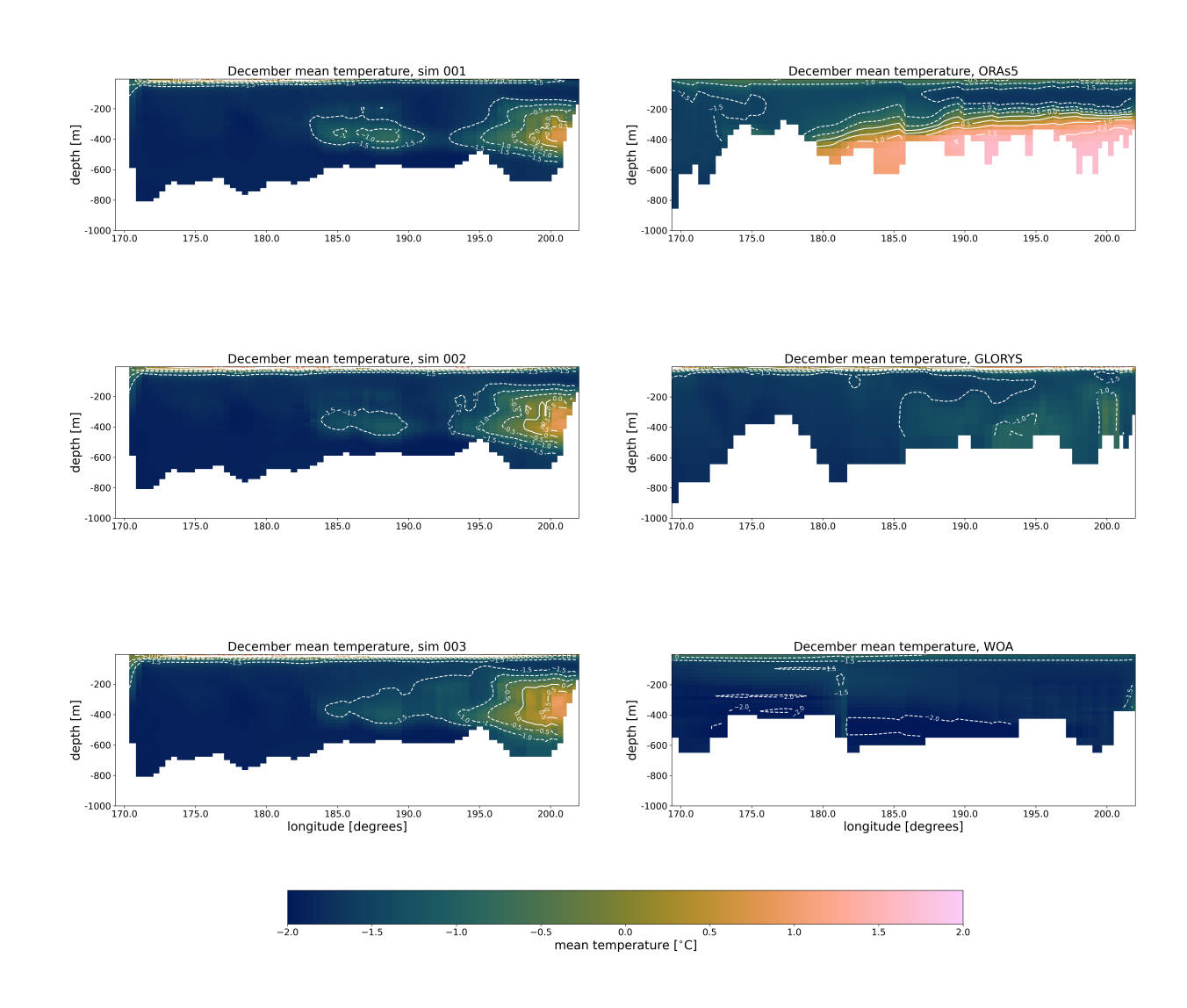


Fig. S11. Temperature profiles and contours along the ice shelf edge, monthly mean values for December 2017.

absent in the Glorys dataset, which has a very confined layer of fresher water at the surface and more saline water in the ERS than in June and does not show much variation across the profile. The December temperature profiles (Figure S11) look similar to the June ones (Figure 13), except for a thin layer of warmer surface temperature in summer. The pockets of warm water inflow in the P-SRKIPS simulations have a larger vertical extent, but are confined around 200° longitude, while the rest of the water is well below 0 °C. ORAs5 has a very similar structure to the mean June profile, with very warm and saline waters sitting at the bottom of the ERS. Both Glorys and WOA show little variation across the profiles and are slightly more homogeneous than in June.

References

185

195

- Bromwich, D. H. and Fogt, R. L.: Strong Trends in the Skill of the ERA-40 and NCEP–NCAR Reanalyses in the High and Midlatitudes of the Southern Hemisphere, 1958–2001, J. Climate, 17, 4603–4619, https://doi.org/https://doi.org/10.1175/3241.1., 2004.
 - Comiso, J. C.: Bootstrap Sea Ice Concentrations from Nimbus-7 SMMR and DMSP SSM/I-SSMIS, Version 3., https://doi.org/https://doi.org/10.5067/7Q8HCCWS4I0R, 2017.
 - Dee, D., Uppala, S., Simmons, A., Berrisford, P., Poli, P., Kobayashi, S., Andrae, U., Balmaseda, M., Balsamo, G., Bauer, P., Bechtold, P., Beljaars, A., van de Berg, L., Bidlot, J., Bormann, N., Delsol, C., Dragani, R., Fuentes, M., Geer, A., Haimberger, L., Healy, S., Hersbach,
- H., Hólm, E., Isaksen, L., Kållberg, P., Köhler, M., Matricardi, M., McNally, A., Monge-Sanz, B., Morcrette, J.-.-J., Park, B.-.-K., Peubey, C., de Rosnay, P., Tavolato, C., Thépaut, J.-.-N., and Vitart, F.: The ERA-Interim reanalysis: configuration and performance of the data assimilation system, O.J.R. Meteorol. Soc., 137, 553–597, https://doi.org/https://doi.org/10.1002/qi.828, 2011.
 - Dee, D. P., Balmaseda, M., Balsamo, G., Engelen, R., Simmons, A. J., and Thépaut, J.: Toward a Consistent Reanalysis of the Climate System, Bull. Amer. Meteor. Soc., 95, 1235–1248, https://doi.org/https://doi.org/10.1175/BAMS-D-13-00043.1., 2014.
- DiGirolamo, N. E., Parkinson, C. L., Cavalieri, D. J., Gloersen, P., and Zwally., H. J.: Sea Ice Concentrations from Nimbus-7 SMMR and DMSP SSM/I-SSMIS Passive Microwave Data, Version 2, https://doi.org/https://doi.org/10.5067/MPYG15WAA4WX, 2022.
 - Fichefet, T. and Maqueda, M. M.: Sensitivity of a global sea ice model to the treatment of ice thermodynamics and dynamics, 102, 12 609–12 646, https://doi.org/doi:10.1029/97JC00480, 1997.
- Fons, S., Kurtz, N., and Bagnardi, M.: A decade-plus of Antarctic sea ice thickness and volume estimates from CryoSat-2 using a physical model and waveform-fitting, The Cryosphere, 17, 2487–2508, https://doi.org/https://doi.org/10.5194/tc-17-2487-2023, 2023.
 - Gasparin, F., Ruggiero, G., Benkiran, M., Drillet, Y., and Le Traon, P.-Y.: The Copernicus Global 1/12° Oceanic and Sea Ice GLORYS12 Reanalysis, Frontiers in Earth Sciences, 9, 2296–6463, https://doi.org/doi.https://doi.org/10.3389/feart.2021.698876, 2021.
 - Huang, B., Liu, C., Banzon, V., Freeman, E., Graham, G., Hankins, B., Smith, T., and Zhang, H.: Improvements of the Daily Optimum Interpolation Sea Surface Temperature (DOISST) Version 2.1., J. Climate, 34, 2923–2939, https://doi.org/https://doi.org/10.1175/JCLI-D-20-0166.1., 2021.
 - Kaleschke, L., Lüpkes, C., Vihma, T., Haarpaintner, J., Bochert, A., Hartmann, J., and Heygster, G.: SSM/I sea ice remote sensing for meoscale ocean-atmosphere interaction analysis, Canad. J. Rem. Sens., 27, 526–537, https://doi.org/https://doi.org/10.1080/07038992.2001.10854892, 2001.
- Kaleschke, L., Tian-Kunze, X., Maaß, N., Mäkynen, M., and Drusch, M.: Sea ice thickness retrieval from SMOS brightness temperatures during the Arctic freeze-up period, Geophysical Research Letters, 39, https://doi.org/10.1029/2012GL050916, 2012.
 - Kaleschke, L., Tian-Kunze, X., Hendricks, S., and Ricker, R.: SMOS-derived Antarctic thin sea ice thickness: data description and validation in the Weddell Sea, Earth System Science Data Discussions, https://doi.org/doi:/https://doi.org/10.5194/essd-2023-326, 2023.
 - Kern, S., Kaleschke, L., and Spreen, G.: Climatology of the Nordic (Irminger, Greenland, Barents, Kara and White/Pechora) Seas ice cover based on 85 GHz satellite microwave radiometry: 1992-2008, Tellus A: Dynamic Meteorology and Oceanography, 62A, 411–434, https://doi.org/https://doi.org/10.1111/j.1600-0870.2009.00457.x, 2010.
 - Madec, G. and Team, T. N.: NEMO Ocean Engine, Note du Pôle de modélisation, 2008.
 - Melsheimer, C. and Spreen, G.: AMSR2 ASI sea ice concentration data, Antarctic, version 5.4 (NetCDF) (July 2012 December 2019), https://doi.org/10.1594/PANGAEA.898400, 2019.

- Powers, J., Monaghan, A., Cayette, A., D.H., B., Kuo, Y.-H., and Manning, K.: Mesoscale modeling over Antarctica: The Antarctic Mesoscale Prediction System (AMPS), Bull. Amer. Meteor. Soc., 84, 1533–1546, https://doi.org/10.1 175/BAMS-84-1 1-153, 2003.
 - Reagan, J., Boyer, T. P., García, H. E., Locarnini, R. A., Baranova, O. K., Bouchard, C., Cross, S., Mishonov, A., Paver, C., Seidov, D., Wang, Z., and Dukhovskoy, D.: World Ocean Atlas 2023, 2024.
 - Sanz Rodrigo, J.: On Antarctic wind engineering, Ph.D. thesis, Université Libre de Bruxelles, 2011.

210

- Spreen, G., Kaleschke, L., and Heygster, G.: Sea ice remote sensing using AMSR-E 89 GHz channels, Journal of Geophysical Research, 113, https://doi.org/10.1029/2005JC003384, 2008.
 - Thompson, L., Smith, M., Thomson, J., Stammerjohn, S., Ackley, S., and Loose, B.: Frazil ice growth and production during katabatic wind events in the Ross Sea, Antarctica, The Cryosphere, 14, 3329–3347, https://doi.org/doi:10.5194/tc-14-3329-2020, 2020.
 - Uotila, P., Goosse, H., Haines, K., Chevallier, M., Barthélemy, A., Bricaud, C., Carton, J., Fučkar, N., Garric, G., Iovino, D., Kauker, F., Korhonen, M., Lien, V., Marnela, M., Massonnet, F., Mignac, D., Peterson, K., Sadikni, R., Shi, L., Tietsche, S., Toyoda, T., Xie, J., and Zhang, Z.: An assessment of ten ocean reanalyses in the polar regions, Climate Dynamics, 52, 1613–1650, https://doi.org/10.1007/s00382-018-4242-z, 2019.
 - Wang, Y., Zhang, X., Ning, W., Lazzara, M. A., Ding, M., Reijmer, C. H., Smeets, P. C. J. P., Grigioni, P., Heil, P., Thomas, E. R., Mikolajczyk, D., Welhouse, L. J., Keller, L. M., Zhai, Z., Sun, Y., and Hou, S.: The AntAWS dataset: a compilation of Antarctic automatic weather station observations, Earth Syst. Sci. Data, 15, 411–429, https://doi.org/https://doi.org/10.5194/essd-15-411-2023, 2023, 2023.
- Zuo, H., Balmaseda, M. A., Tietsche, S., Mogensen, K., and Mayer, M.: The ECMWF operational ensemble reanalysis—analysis system for ocean and sea ice: a description of the system and assessment, Ocean Sci., 15, 779–808, https://doi.org/https://doi.org/10.5194/os-15-779-2019, 2019.